STATISTICAL MODELLING AND MECHANICAL BEHAVIOUR OF LATERITE NANOPARTICLES REINFORCED A356 ALUMINIUM ALLOY COMPOSITE

Abdulhamid, S.[1*], Muhammad, M.H.[2], Bawa, M.A.[2] and Abioye, A.M.[2]

[1]Department of Mechanical Engineering, Modibbo Adama University Yola, Nigeria

[2]Department of Mechanical/Production Engineering, Abubakar Tafawa Balewa University Bauchi, Nigeria

*Corresponding email: sabdulhamid@mau.edu.ng

ABSTRACT

The increasing demand for cost effective and sustainable reinforcement materials in advanced engineering applications has stimulated interest in the utilization of naturally abundant resources such as laterite. The present research investigates the mechanical properties (tensile and impact strength) of laterite nanoparticles reinforced A356 aluminium alloy composite using a double stir casting process. Laterite nanoparticles with an average particle size of 27.37 nm were incorporated into the aluminium matrix to enhance its mechanical performance. The influence of processing parameters; pouring temperature (720°C, 740°C and 760°C), stirring speed (200rpm, 400rpm and 600rpm) and reinforcement composition (2, 4 and 6 wt%) on the composite properties were evaluated using Box-Behnken Design (BBD) and Response Surface Methodology (RSM) in Design Expert software (version 13). The developed composites were characterized through tensile and impact strength while microstructural features were examined using scanning electron microscopy (SEM). The results revealed that, the tensile strength increases as the reinforcement content rises from lower levels (2 wt.%) to an optimal range of 3.5-4.5 wt.%, and beyond this optimal reinforcement level, a decline in tensile strength was observed. Also, as the temperature increases from 720 °C to an intermediate range of 740-750 °C, tensile strength improves significantly. Impact strength showed moderate improvement at 2 wt.% reinforcement at pouring temperatures of 730-745 °C with intermediate stirring speeds of 350-450 rpm, as the reinforcement percentage increases from 2 to 6 wt%, a gradual decline in impact strength was observed. The optimization process identified the optimal conditions as 760 °C pouring temperature, 600 rpm stirring speed and 2.802 wt.% reinforcement. Under these conditions, the predicted properties were 243.079 N/mm² tensile strength and 54.676 kJ/m² impact strength. These values correspond to improvements of 45.45 % and 27.06 % in tensile and impact strength respectively, compared to the unreinforced alloy. Microstructural analysis confirmed a relatively uniform dispersion of laterite nanoparticles within the matrix, which contributed to the enhancement of mechanical properties. Validation experiments were conducted at the optimized conditions, which showed good agreement with the predicted results, with minimal percentage errors of 2.48 % and 4.46 % for tensile and impact strength respectively. Since all errors were below 5%, the developed models were deemed statistically reliable and adequate for predicting the composite performance. The outcome of the research showed that, laterite nanoparticles is a viable and sustainable reinforcement material for aluminium matrix composites.

Keywords: Aluminum, Laterite nanoparticles, Sand Casting, Response Surface Methodology

1 INTRODUCTION

The development of Aluminium Metal Matrix Composites (Al-MMCs) is attracting much attention owing to their low weight and enhanced mechanical properties [1, 2]. Metal Matrix Composites (MMCs) have attractive combination of properties like high specific modulus and strength, enhanced elevated temperature properties, wear resistance and good abrasion resistance properties [3, 4, 5]. Due to these attractive properties, MMCs are being considered for a wide range of applications in space shuttles, commercial airliners, electronic substrates and automobiles [6, 7]. Particulate reinforced Al-MMCs are engineered combination of aluminium metal/alloy with particles, whiskers or short fiber reinforcement. Al-

MMCs are reinforced with particles of various sizes, ranging from micro to Nano sizes [8]. Nano particle refers to a particle with any of its dimension less than 100nm (Nano meters). Metal Matrix Composites (MMCs) reinforced with micro sized particles are classified as micro-composites, while those reinforced with Nano size particles are classified as Nano-composites. The properties of Al-MMCs can be enhanced significantly without much increase in weight when reinforced with nanoparticles, as compared with those reinforced with micro sized particles [9, 10]. Hence, most researches for the advancement of MMCs are focusing on the development of metal matrix Nano-composites (MMNCs) [11]. Proper incorporation of reinforcements in the matrix and excellent mechanical properties can be obtained by selecting appropriate process parameters; such as the nature of the reinforcement, casting temperature and stirring parameters [12, 13]. However, the greatest challenges facing the development of MMCs for wide application are the high cost of effective reinforcements and the cost and complexity of its synthesis [14]. In an attempt to address these problems, researches are exploring the use of industrial by product and naturally occurring materials such as granite and clay as reinforcements because of their low cost or availability in large quantity [14]. Laterite is a group of highly weathered soil formed by the concentration of hydrated oxides of iron, and aluminium [15]. Laterites and lateritic soils form a group comprising a wide variety of red, brown, and yellow fine-grained residual soils of light texture as well as nodular gravels and cemented soils indicating the presence of iron oxide which makes laterite chemically written as Fe_2O3-Al_2O_3-SiO_2-H_2O [16]. The term Laterite is derived from the Latin word 'later' meaning brick. It was first used in 1807 by Buchanan to describe a red iron-rich material found in the southern part of India. Laterites are widely distributed throughout the world in the regions with high rainfall, especially in the inter-tropical areas of Africa, Australia, India, South-East Asia, and South America where they are generally present just below the surface of grasslands or forest clearings [15]. In the present investigation, an attempt is made to utilize laterite nanoparticles of an average particles size of 27.23nm as reinforcement in A356 aluminium alloy.

2 EXPERIMENTAL PROCEDURES

2.1 Materials and Equipment

The materials and equipment used in this study include: Laterite source from Kofar Kona (11.05283^o, 7.78321^o) Zaria, Kaduna state, Nigeria, A356 aluminium alloy, ceramic jar, ceramics balls, ethanol, spoons, trays, furnace, digital weighing balance, Laboratory crusher, Drying oven, Ball milling machine, X-ray fluorescence (XRF), Dynamic Light Scattering (DLS) particles size analyzer and Scanning Electron Microscope (SEM) machine. Table 1 shows the X-ray Fluorescence (XRF) analysis of laterite nano particulate. It is a mineral having a high composition predominantly of silica (SiO_2), alumina (Al_2O_3), and iron oxide (Fe_2O_3), with minor constituents including titanium dioxide (TiO_2) and trace elements such as K_2O, CaO, ZrO_2, SO_3 and V_2O_5. These results are in agreement with earlier observation of [16, 26].

Table 1. Chemical Composition of the Laterite Nanoparticles

Constituents	SiO_2	Al_2O_3	Fe_2O_3	TiO_2	K_2O	CaO	ZrO_2	SO_3	V_2O_5	others
Composition (wt.%)	56.31	26.06	11.77	2.00	1.74	0.40	0.19	0.16	0.11	1.23

DLS analysis revealed an average particle size of 27.37 nm, confirming that the particles lie within the nanometer range (< 100 nm). The polydispersity index (PDI) of 0.212, indicating a moderate level of polydispersity (moderate uniform size distribution). According to ISO 22412 [27] and ASTM E3247-20 [28], PDI value below 0.30 are considered acceptable for nanoparticle systems, though values below 0.1 indicate highly monodisperse suspensions.

2.2 Fabrication of A356/Laterite nanoparticles Composite

The A356/laterite nanoparticle reinforced composites were produced using the double stir casting technique in the order of the works of [17, 18, 19] was adopted due to its effectiveness in enhancing the uniform distribution of reinforcement particles, improving wettability, and minimizing agglomeration, which are common challenges in conventional stir casting, especially when dealing with nanoparticles. Each weight percent of the Aluminium, Silicon, Magnesium and Laterite nanoparticles required to produce the melts were obtained through charge calculation. The control sample was the unreinforced aluminium alloy, while the developed composite compositions with corresponding designations are presented in Table 3. The aluminium, silicon powder, and magnesium were accurately measured based on the target composition. The aluminium metal was first charged into a pre-heated graphite crucible to minimize thermal shock and contamination. The crucible containing the aluminium charge was placed in charcoal crucible furnace and heated to a temperature of 750°C, which is above the melting point of aluminium to ensure complete liquefaction and adequate superheat for alloying. Once the aluminium was fully molten, the pre-weighed silicon powder was gradually added to the melt. After thorough stirring to facilitate dissolution and homogenization, magnesium was introduced into the melt. Stirring continued for 6 minutes to ensure uniform distribution of the alloying elements. The laterite nanoparticles, previously synthesized via ball milling, were oven-dried and preheated at a temperature of 400°C for about 2 hours. This preheating step was necessary to remove moisture, improve wettability between the particles and molten aluminium, and minimize the temperature gradient during addition into the melt. With the liquid Al-7%Si-0.3%Mg alloy still in the crucible at 750°C, it was allowed to cool gradually to a temperature of 605°C (which is 15 °C below the liquidus temperature). This is to keep the alloy as close as possible in a semi-solid state before incorporating the reinforcement particles into the melt. After which, the pre-heated laterite nanoparticles were added at this temperature, and stirred manually in the semi - solid melt for 5 minutes. The composite slurry was then superheated at 720, after which a second stirring was performed on the mixture using a mechanical stirrer for another 6 minutes in order to disperse the particles in the melt. This process was repeated with different weight percentages of laterite nanoparticles (2, 4 and 6wt.%), and different stirring speed of (200rpm, 400rpm, 600rpm). After the reinforcement was introduced, the melt was heated up again to a temperature above the melting point (viz: 720°C, 740°C, 760°C) and the melt temperature was controlled before casting. The molten composite was then cast into molding sand and allowed to solidify. The choice of sand casting as the fabrication route was as a result of its flexibility and ease of operation. Several authors had also adopted the technique in the fabrication of aluminium-based composites [20, 21].

2.3 Mechanical and Morphological Characterization

2.3.1 Tensile Test

Electronic Universal Testing Machine (Model WDW-100KN, Serial:190536) was used to perform the tensile test as shown in Figure 1B, and the tensile test samples is presented in Figure 1A. The specifications of the machine include a load resolution of 0.5 mN and the minimum displacement rate of 0.001 mm/min. To avoid the effect of strain rate, a fixed strain rate of 2.764 x10^{-3} s^{-1} was used for all tests. All testing was conducted at ambient temperature. The diameter was measured by the customary optical diffractometer, where a 532-nm green laser was used. The test method adopted was ASTM E8 [22]. The machined sample was mounted at its ends onto the holding grips of the extensometer. The stress-strain and percentage elongation graphs were digitally obtained from the computer connected to the machine.

Figure 1. Represent (A) Tensile test samples and (B) Electronic universal tensile test machine

2.3.2 Impact Test

The toughness was determined using Charpy impact testing machine (model no.: HD96QD, serial no.: 412-07-15269C) with capacity of 15J-25J. The impact test samples and Charpy impact testing machine is shown in Figure 1A and B. The test method adopted was in accordance with ASTM E23 [23]. Before the test, the pendulum was set to a potential energy position. The test sample was griped vertically in a vice, the trigger was released and the registering pointer of the quadrant scale indicated the energy absorbed in Joules in breaking the sample. The energy absorbed was recorded. Impact strength (energy absorbed per unit area under the notch) was calculated from the impact energy and the sample dimension. The same process was repeated for other test pieces.

Figure 2. Represent (A) Impact test samples and (B) Charpy Impact Testing Machine

2.3.3 Microstructural Analysis

All the specimens were prepared for scanning electron microscope (SEM) using the standard metallographic techniques. The specimens were grounded on a water lubricated silicon carbide abrasive papers of 180, 240, 320, 400 and 600 grade sizes. Polishing was carried out on two 15cm rotating discs of a METASERV universal polishing machine with synthetic velvet polishing clothes impregnated with 1-micron Alumina paste. The specimens were etched with Keller's reagent solution using the swabbing method with cotton wool soaked in the etchant.

2.4 Experimental Design

The experiments were planned based on Response surface methodology (RSM) employing a Box-Behnken Design (BBD) method in Design Expert software (Version 13), were used to optimize the mechanical attributes of laterite nanoparticles materials. It utilized three (3) independent factors and three level design schemes as shown in Table 2. The factors are; A-Pouring Temperature (°C), B-Stirring Speed (rpm) and C-Reinforcement (wt. %).

Table 2. Factors and their levels used in Box-Behnken Design Matrix

Level	A-Pouring Temperature T(°C)	B-Stirring Speed (rpm)	C-Reinforcement L (wt%)
1	720	200	2
2	740	400	4
3	760	600	6

Based on the BBD, a total of 17 experimental runs were obtained. Five (5) replicate center points were included to capture experimental noise and to test the goodness of fit of the quadratic model [24, 25]. The optimization responses focused on the tensile and impact strength of the composites. The experimental data were fitted to a second-order polynomial regression, and the adequacy of the model was tested using ANOVA. The experimental outcome is presented in Table 3.

Table 3. Box-Behnken Design (BBD) matrix and responses for laterite nanoparticles reinforced A356 matrix composite

Expt. Runs	A: Pouring Temperature (°C)	B: Stirring Speed (rpm)	C: Weight Reinforcement (L %)	Tensile Strength (N/mm^2)	Impact Strength (KJ/m^2)
1	760	200	4	227.00	41.00
2	740	200	2	209.20	50.40
3	760	600	4	253.70	45.00
4	720	400	2	220.33	55.30
5	740	400	4	249.40	42.50
6	760	400	2	216.60	57.20
7	740	400	4	241.25	43.00
8	740	400	4	239.40	43.90
9	740	600	2	215.00	59.80
10	740	600	6	213.30	31.60
11	720	200	4	240.80	42.00
12	760	400	6	201.70	33.90
13	740	400	4	238.22	42.60
14	720	600	4	250.40	44.00
15	720	400	6	194.30	32.80
16	740	400	4	223.00	42.30
17	740	200	6	183.60	34.00

3 RESULTS AND DISCUSSION

3.1 Characterization of As-cast A356 Alloy

The SEM micrograph of the as-cast A356 alloy in Figure 3 (a) reveals the structure of the eutectic phase containing Mg_2Si in α-aluminium matrix. The Mg and Si in the A356 alloy are present as a solid solution phase in the grains and along the grain-boundaries. The prominent peaks corresponding to aluminium, magnesium and silicon in the A356 alloy is confirmed by the energy dispersive spectroscopy (EDS) spectra shown in Figure 3 (b). Aluminium is observed to have the highest count than other elements present.

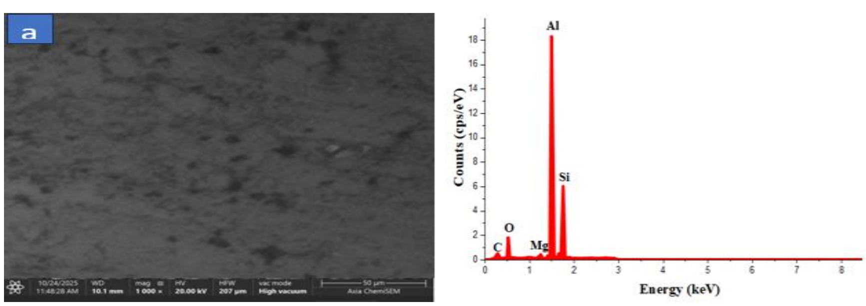

Figure 3: (a) SEM/EDS spectrum of the aluminium alloy

3.3 Mathematical Model Development

For model development, the mathematical relationship between the response and the input factors is expressed by the second order polynomial in eqn. 1: From the equation, Y represents the response, Xi and Xj are the equation value of the factors, β0 is the constant, βi, βj and βij are linear, interaction and quadratic end coefficient respectively, k is the number of the factors and ε is the random error term. The experimental results generated after conducting the runs were analyzed using analysis of variance (ANOVA) to confirm the adequacy and validity of the developed model considering the significant model terms. The adequacy and validity are ascertained by confirming the significant terms with p values < 0.05 while model terms with p values > 0.05 are considered insignificant [29].

$$Y = \beta_0 + \sum_{i=1}^{k} \beta_i x_i + \sum_{i=1}^{k} \beta_{ii} x_i^2 + \sum_{i<j}^{k} \beta_{ij} x_i x_j + \varepsilon \quad (1)$$

3.4 Model for Tensile Strength of the developed Composite

Fit summary statistics of the model for tensile strength is shown in Table 4. The fit summary presents the models to fit experimental data into appropriate model equations which can be first order or linear, second order or quadratic and cubic. From the table, the suggested polynomial for tensile strength with F-value of 27.22 at p-value 0.0003 is significant and quadratic.

Table 4. Fit summary statistics for tensile strength

Source	Sum of Squares	df	Mean Square	F-value	p-value	
Mean	8.57E+05	1	8.57E+05			
Linear	1232.15	3	410.72	0.9689	0.4369	
2FI	246.87	3	82.29	0.1563	0.9232	
Quadratic	4848.06	3	1616.02	27.22	0.0003	Suggested
Cubic	48.4	3	16.13	0.1757	0.9076	Aliased
Residual	367.21	4	91.8			
Total	8.64E+05	17	50815.37			

Analysis of variance (ANOVA) for tensile strength carried out at 5 % significance level is presented in Table 5. It is observed from the table that the model is significant with a p-value of 0.0018 which is less than 0.05 and F-value of 11.84. P-values less than 0.0500 indicate model terms are significant. In this case, B, C and C^2 are statistically significant model terms since their p-values are less than 0.05 while, AB, AC, BC, A^2 and B^2 are insignificant model term. Furthermore, the p-value of the lack of fit which corresponds to 0.9076 is greater than 0.05 indicating that the lack of fit is non-significant which is desirable for model adequacy.

Table 5. Analysis of Variance (ANOVA) for Tensile Strength

Source	Sum of Squares	df	Mean Square	F-value	p-value	
Model	6327.09	9	703.01	11.84	0.0018	significant
A-Pouring Temperature (°C)	5.83	1	5.83	0.0982	0.7631	non-significant
B-Stirring Speed (rpm)	644.41	1	644.41	10.85	0.0132	significant
C-Reinforcement (%)	581.92	1	581.92	9.80	0.0166	significant
AB	73.10	1	73.10	1.23	0.3038	non-significant
AC	30.97	1	30.97	0.5216	0.4936	non-significant
BC	142.80	1	142.80	2.41	0.1649	non-significant
A^2	62.06	1	62.06	1.05	0.3406	non-significant
B^2	3.27	1	3.27	0.0551	0.8211	non-significant
C^2	4827.58	1	4827.58	81.31	< 0.0001	significant
Residual	415.61	7	59.37			
Lack of Fit	48.40	3	16.13	0.1757	0.9076	not significant
Pure Error	367.21	4	91.80			
Cor Total	6742.70	16				

$R^2 = 0.9384$ $R^2(adj) = 0.8591$ $R^2(pred) = 0.8001$

Also, the difference between the predicted R^2 (0.8001) and adjusted R^2 (0.8591) of the model is less than 0.2, which establishes the reasonable agreement required for model adequacy. The model equation developed for the prediction of tensile strength for any given level of each of the process parameters in the experiment is presented in equations 2.

$$Tensile\ Strenght = 238.25 - 0.8538A + 8.98B - 8.53C + 4.28AB + 2.78AC + 5.98BC + 3.84A^2 + 0.8817B^2 - 33.86C^2 \quad (2)$$

It was apparent that there were terms that might be eliminated to increase the accuracy of the model. The non-significant terms were automatically reduced by a backward elimination process, and the resulting model equation is given by equation 3.

$$Tensile\ Strenght = 238.25 + 8.98B - 8.53C - 33.86C^2 \quad (3)$$

3.4.1 Effect of Process Parameters on Tensile Strength

Figure 4 displays the 3D surface plot for the interaction between pouring temperature (A), stirring speed (B), and reinforcement content (C). It’s demonstrated that, the tensile strength was significantly influenced by their interaction. Tensile strength increased with increasing stirring speed up to an optimal range of 400–500 rpm due to improved dispersion of laterite nanoparticles and enhanced interfacial bonding [30]. Similarly, reinforcement content improved tensile strength up to approximately 3.5-4.5 wt.% through dispersion strengthening, after which agglomeration and poor wettability caused a decline in performance, this is in agreement with observation of [30]. Pouring temperature also enhanced tensile strength as it increased from 720 °C to an optimum range of 740–750 °C by improving melt fluidity and particle wettability. Beyond the optimum temperature and reinforcement levels, tensile strength decreased due to oxidation, gas absorption, porosity, and particle clustering [31]. The highest tensile strength values (approximately 250-253 N/mm²) were obtained at moderate-to-high stirring speeds, intermediate pouring temperatures, and reinforcement contents of about 3.5-4.5 wt.%, as confirmed by the elliptical contour plots indicating strong parameter interactions.

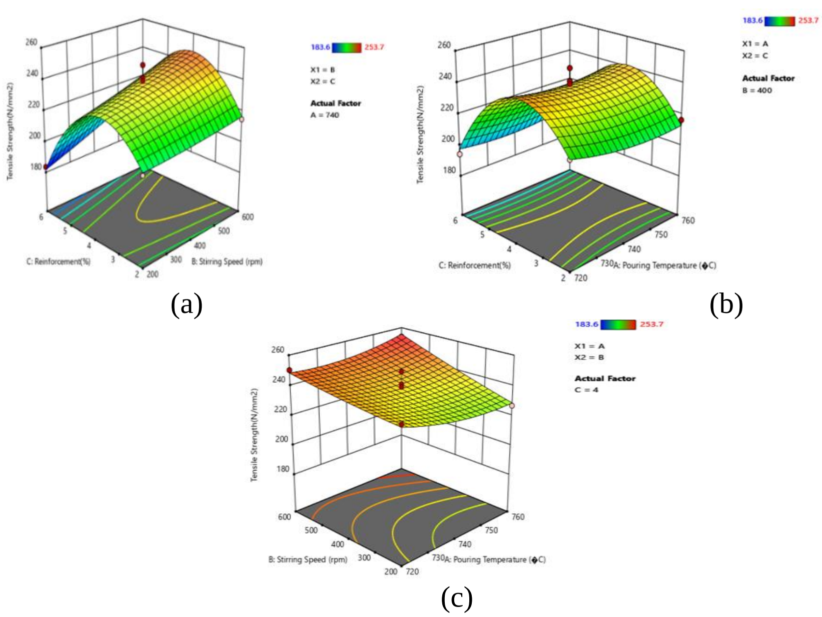

Figure 4. 3-D surface plots of tensile strength based on various process parameters (a) stirring speed versus reinforcement (b) pouring temperature versus reinforcement (c) pouring temperature versus stirring speed

4.5 Model for Impact Strength of the developed Composite

Fit summary statistics of the model for impact strength is shown in Table 6. From the table, the suggested quadratic polynomial for coefficient of friction has F-value of 8.00 at significant p-value of ≤ 0.0116. Analysis of variance (ANOVA) for coefficient of friction carried out at 5 % significance level is presented in Table 7. From the table, it is observed that the model is significant with a p-value of 0.0001 which is less than 0.05 and F-value of 278.73. In this case, B, C, BC and C^2 are statistically significant model terms since their p-values are less than 0.05. Values greater than 0.05 indicate the model terms are not significant. If there are many insignificant model terms (not counting those required to support hierarchy), model reduction may improve the model. Furthermore, the p-value of the lack of fit which corresponds to 0.4215 is greater than 0.05 indicating that the lack of fit is non-significant which is desirable for model adequacy. Also, the difference between the predicted R^2 (0.9768) and adjusted R^2 (0.9936) of the model is less than 0.2, which establishes a reasonable agreement as required for model adequacy.

Table 6. Fit summary statistics for impact strength

Source	Sum of Squares	df	Mean Square	F-value	p-value	
Mean	32325.04	1	32325.04			
Linear	1043.77	3	347.92	91.49	< 0.0001	
2FI	35.97	3	11.99	8.90	0.0036	
Quadratic	**10.43**	**3**	**3.48**	**8.00**	**0.0116**	**Suggested**
Cubic	1.43	3	0.4767	1.18	0.4215	Aliased
Residual	1.61	4	0.4030			
Total	33418.25	17	1965.78			

Equation 4 is the model equation developed for the prediction of impact strength for any given level of each of the process parameters in the experiment. The relative influence of processing parameters on impact strength is identified by comparing their coefficients using equation 5. From the equation, it is concluded that the process parameter with the most influence on impact strength is reinforcement fraction.

$$Impact\ Strenght = 42.86 + 0.3750A + 1.63B - 11.30C + 0.5AB5 - 0.2AC - 2.95BC + 0.4950A^2 - 0.3550B^2 - 1.45C^2 \quad (4)$$

$$Impact\ Strenght = 42.86 + 1.63B - 11.30C - 2.95BC - 1.45C^2 \quad (5)$$

Table 7. Analysis of Variance (ANOVA) for Impact Strength

Source	Sum of Squares	df	Mean Square	F-value	p-value	
Model	1090.17	9	121.13	278.73	< 0.0001	significant
A-Pouring Temperature (°C)	1.13	1	1.13	2.59	0.1517	non-significant
B-Stirring Speed (rpm)	21.13	1	21.13	48.61	0.0002	significant
C-Reinforcement (%)	1021.52	1	1021.52	2350.64	< 0.0001	significant
AB	1	1	1	2.3	0.1731	non-significant
AC	0.16	1	0.16	0.3682	0.5632	non-significant
BC	34.81	1	34.81	80.1	< 0.0001	significant
A^2	1.03	1	1.03	2.37	0.1673	non-significant
B^2	0.5306	1	0.5306	1.22	0.3057	non-significant
C^2	8.79	1	8.79	20.23	0.0028	significant
Residual	3.04	7	0.4346			
Lack of Fit	1.43	3	0.4767	1.18	0.4215	not significant
Pure Error	1.61	4	0.403			
Cor Total	1093.21	16				

R^2 = 0.9972 *R^2(adj) = 0.9936* *R^2(pred) = 0.9768*

3.5.1 Effect of Process Parameters on Impact Strength

Figure 5a displays the response surface plot for the combined effect of stirring speed (B) and reinforcement (C) on the tensile strength of the developed composite while holding the pouring temperature (A) constant at 740°C. increasing reinforcement content from 2 to 6 wt.% resulted in a gradual reduction in impact strength due to increased brittleness, particle clustering, and stress concentration effects. Similar observations were reported by [32, 14]. Stirring speed positively influenced impact strength, as higher speeds (500–600 rpm) promoted uniform particle dispersion and stronger matrix reinforcement bonding. The highest impact strength of 59.80 KJ/m^2 was achieved at high pouring temperatures, high stirring speeds and low reinforcement contents (2-3 wt.%), while the lowest values occurred at low stirring speeds combined with high reinforcement levels. Figure 6b depicts the response surface plot showing the combined influence of pouring temperature (A) and reinforcement content (C) on the impact strength of the developed composite at a constant stirring speed 0f 400rpm. It's revealed that, a clear linear and positively sloped trend is observed along the pouring temperature axis, indicating that impact strength increases significantly with increasing pouring temperature within the range (720-760°C). Figure 6c shows the interaction between pouring temperature and stirring speed with reinforcement relatively constant at 4 wt%, showing only slight improvement at moderate temperatures (730-745°C) and stirring speeds (350-450 rpm). Pouring temperature had a positive effect on impact strength, with higher temperatures (up to 760°C) enhancing melt fluidity, wettability, and interfacial bonding, thereby improving energy absorption capacity.

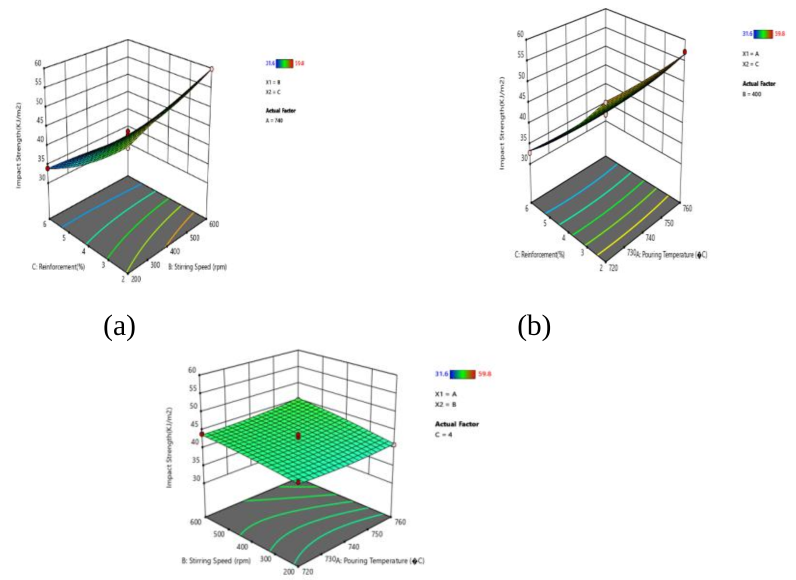

(a) (b) (c)

Figure 5. 3D surface plot of impact strength based on various process parameters (a) stirring speed versus reinforcement (b) pouring temperature versus reinforcement (c) pouring temperature versus stirring speed

4 MULTI-OBJECTIVE OPTIMIZATION ANALYSIS AND RESULT VALIDATION

The two models obtained in equation 3 and 5 can be used to generate points of desirable results in the design region for tensile and impact strength respectively, since the required process condition for one response is different from the other. Therefore, this can be overcome through utilization of multi-objective optimization (MOO), to obtain a set of process conditions through which all responses can be simultaneously optimized. Optimization was affected with the response surface method via the engagement of Design Expert Software (version 13) similar to [33, 29]. For this study, the goal (is to maximize and set in range), lower and upper limits for optimizing the responses. Based on the solution analysis in Table 8, optimum values of input process parameters are achieved with experiment number 1 and the ramp graph showing the details of the input factors and the corresponding responses is shown in Figure 7. From Table 8 and Figure 6, the optimum influence of processing parameters on the mechanical behaviour of the composites obtained from the MOO are 2.802 wt% reinforcement, 760 °C pouring temperature and 600. rpm stirring speed. The resulting responses at this optimized condition are 243.079 N/mm^2 for tensile strength and 54.676 KJ/m^2 for impact strength with a confidence and desirability level of 0.816.

Table 8. Optimal Solutions generated for the responses

S/N	A	B	C	Tensile Strength (N/mm^2)	Impact Strength (KJ/m^2)	Desirability	
1	**760.000**	**600.000**	**2.802**	**243.079**	**54.676**	**0.816**	**Selected**
2	760.000	599.997	2.779	242.611	54.860	0.816	
3	760.000	599.723	2.815	243.336	54.563	0.816	
4	760.000	600.000	2.847	243.978	54.314	0.816	
5	759.921	600.000	2.762	242.216	54.991	0.816	

A=Pouring Temperature (°C), B=Stirring Speed (rpm) and C=Reinforcement (wt%)

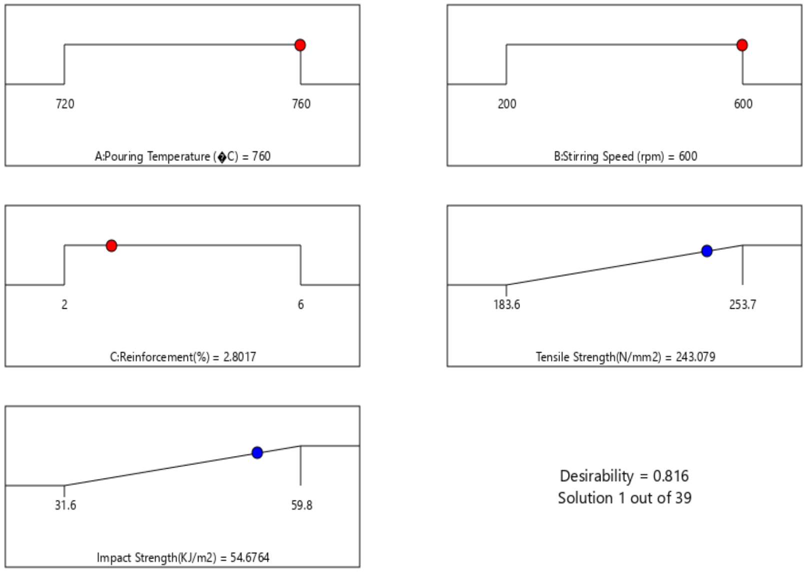

Figure 6. Ramp graph at optimal solution

4.1 Confirmation Test (Validation)

To validate the predicted outcome, samples were prepared at optimum conditions and tested for their responses. Three specimens were prepared for each of the respective tests, and the mean results were recorded for each response. The validation procedure yielded the following results: 249.258 N/mm^2 (2.48 % error) and 52.235 KJ/m^2 (4.46 % error) for tensile and impact strength, respectively. Since the errors for each of the responses is less than 5%, therefore there is no significant discrepancy between the predicted outcome and the experimental outcome. Hence, the models are certified as statistically competent in the prediction of the property responses. The confirmation test result is presented in Table 9.

Table 9. Confirmatory test result of the optimized parameters

Predicted optimal conditions for responses					
Pouring Temperature (°C)	Stirring Speed (rpm)	Reinforcement (wt%)	Tensile Strength (N/mm^2)	Impact Strength (KJ/m^2)	
760.000	600.000	2.802	243.079	54.676	
Actual experiments (validations)					
		Actual	Predicted	Deviation	
TS1 (N/mm^2) 248.865	TS2 (N/mm^2) 247.056	TS3 (N/mm^2) 251.854	Mean TS (N/mm^2) 249.258	TS (N/mm^2) 243.079	2.48 %
IS1 (KJ/m^2) 53.822	IS2 (KJ/m^2) 52.961	IS3 (KJ/m^2) 49.922	Mean IS (KJ/m^2) 52.235	IS (KJ/m^2) 54.676	4.46 %

TS = Tensile strength *IS = Impact strength*

4.2 Microstructural Analysis of the Confirmation Test Sample

The microstructural features of a sample prepared at optimum conditions is presented in Figure 7, which demonstrated how the particles are uniformly disperse at the stipulated dosages in the matrix. The matrix reveals no significant presence of intermetallic phases as well as micro-pores. Similar observations were made by [34, 35].

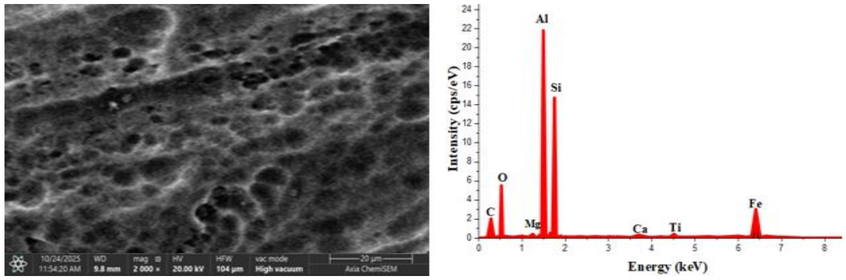

Figure 7. SEM/EDS spectrum of A356/Laterite nanoparticles at optimum conditions.

5 CONCLUSIONS

Based on the results of this study, the following conclusions can be drawn: The composite, Al-7%Si-0.3%Mg/Laterite nano particles were successfully developed via double stir casting process route. The addition of laterite nanoparticles significantly improved the mechanical properties of the base alloy. Notable enhancements were observed in tensile strength, confirming the strengthening potential of laterite as a reinforcement material. Tensile strength increases as the reinforcement content rises from lower levels (2 wt.%) to an optimal range of 3.5-4.5 wt.%, and beyond this optimal reinforcement level, a decline in tensile strength was observed. Also, as the temperature increases from 720 °C to an intermediate range of about 740-750 °C, tensile strength improves significantly. Impact strength showed moderate improvement at 2 wt.% reinforcement at pouring temperatures (around 730-745 °C) with intermediate stirring speeds (approximately 350-450 rpm), as the reinforcement percentage increases from 2 to 6 wt%, a gradual decline in impact strength was observed. Response Surface Methodology (RSM) and Box-Behnken Design (BBD) successfully modelled and optimized the process parameters, establishing reliable predictive relationships between inputs and responses. The surface plots revealed that the responses were influenced by the interaction effects among the process variables. The optimum processing conditions were obtained as 760 °C pouring temperature 600 rpm stirring speed and 2.802 wt.% reinforcement and the predicted values of responses at that condition were 243.079 N/mm^2 and 54.676 KJ/m^2 for tensile and impact strength respectively. Confirmation results for the responses are 249.258 N/mm^2 (2.48 % error) and 52.235 KJ/m^2 (4.46 % error) for tensile and impact strength respectively. The deviation for each response is less than 5%, thereby validating the models. Validation experiments showed close agreement with predicted results, confirming the statistical adequacy and reliability of the developed models. The morphology of the optimized specimen revealed dispersion of laterite nanoparticles within the matrix at optimal conditions, with minimal agglomeration and improved interfacial bonding.

REFERENCES

1. Kar, A., Sharma, A. and Kumar, S. (2024). A critical review on recent advancements in aluminium-based metal matrix composites. *Crystals*, vol. 14, no. 5, pp. 412-425.
2. Yadav, A. and Dubey, A.K. (2026). Investigating Mechanical and Microstructural Characteristics of Aluminium Metal Matrix Composites (Al-MMC) Fabricated via Two-step Stir Casting Technique. *Transactions of the Indian Ceramic Society*, pp. 1-12.
3. Bawa, M.A., Umaru, O.B., Abur, B.T., Salako, I. and Jatau, J.S. (2020). Effect of Locust Bean Pod Ash on the Hardness and Wear Rate of Heat Treated A356 Alloy Metal Matrix Composite for Production of Automobile Brake Rotor. *International Journal of Research Publications*, vol.-57, issue-1, pp. 2708-3578.
4. Suneev, A.B., Virat, K. and Pallav, G. (2022). Metal Matrix Composite: Properties and Application, *CRC Press*, vol. 2, no. 1, pp. 27-49.
5. Patel, S.K. and Shi, L. (2025). Recent advances in ceramic-reinforced aluminum metal matrix composites: a review. *Alloys*, vol. 4, no. 3, pp. 18-31.
6. Divya Deepak, G., Kashimat, N., Birru Manjunathaiah, K., Nayak, V., Anne, G. and Sharma, S. (2025). Optimizing the Tribological Performance of Copper-Reinforced A356 Aluminium Alloy:

Influence of Heat Treatment and Composition Variation. *Journal of Composites Science*, vol. 9, no. 6, pp. 287-299.

7. Kumar S, Theerthan J.A. (2008). Production and characterization of aluminium-fly ash composite using stir casting method (PhD dissertation). Rourkela: *National Institute of Technology*, pp. 87-91
8. Srivastava, A.K., Sharma, B., Saju, B.R., Shukla, A., Saxena, A. and Maurya, N.K. (2020). Effect of Graphene nanoparticles on microstructural and mechanical properties of aluminium-based nanocomposites fabricated by stir casting. *World Journal of Engineering*, vol. 17, no. 6, pp. 859-866.
9. Ghahremani, A., Abdullah, A., Fallahi Arezoodar, A. and Gupta, M. (2023). An investigation on the enhanced wear behaviour of ultrasonically stirred cast A356/SiO2np nano-composites. *Crystals*, vol. 13, no. 5, pp. 722-739.
10. Saputri, T.K., Zulfia, A. and Hernandha, R.F.H. (2025). Strontium-based additive for enhanced aluminium A356-reinforced Al2O3 composite mechanical properties and microstructures. *Metallurgical Research & Technology*, vol. 122, no. 1, pp. 112-123.
11. Al Mahmoud, Z., Safaei, B., Asmael, M., Kenevisi, M.S., Sahmani, S., Karimzadeh, S. and Hui, D. (2025). Impact of process parameters on mechanical and microstructure properties of aluminum alloys and aluminum matrix composites processed by powder-based additive manufacturing. *Journal of Manufacturing Processes*, vol. 146, pp. 79-158.
12. Sozhamannan, G.*G*.S., BalasivanandhaPrabu, V.S.K. Venkatagalapathy (2012). Effect of Processing Parameters on Metal Matrix Composites: Stir Casting Process. *Journal of Surface Engineered Materials and Advanced Technology*, vol. 2, pp. 11-15.
13. Alem, S.A.A., Sabzvand, M.H., Govahi, P., Poormehrabi, P., Hasanzadeh Azar, M., Salehi Siouki, S. and Bagherifard, S. (2025). Advancing the next generation of high-performance metal matrix composites through metal particle reinforcement. *Advanced composites and hybrid materials*, vol. 8, no. 1, pp. 31-45.
14. Dodo, R.M., Abdulwahab, M., Abdullahi, A. and Saeed, A.I. (2018). Effect of granite particles size on the properties of Al-7%Si-0.3%Mg/Granite particulate composite. *Silicon (springer)*, vol. 10, no. 5, pp. 2211-2217.
15. Ozigi, P.B.., Tuleun, L.Z. and Jimoh, A.A. (2020). Flexural Strength Behaviour of APA (Afzeliabipindensis) Reinforced Stabilized Lateritic Soil Beam. *Civil Engineering Dimension*, vol. 22, no. 1, pp. 22-28.
16. Kaze, C.R., Lecomte-Nana, G.L., Kamseu, E., Camacho, P.S., Provis, J.L., Duttine, M. and Melo, U.C. (2021). Mechanical and physical properties of inorganic polymer cement made of iron-rich laterite and lateritic clay: A comparative study. *Cement and Concrete Research*, vol. 140, pp. 106-129.
17. Jayaprakash, D., Niranjan, K. and Vinod, B. (2023). Studies on mechanical and microstructural properties of aluminium hybrid composites: influence of SiC/Gr particles by double stir-casting approach. *Silicon*, vol. 15, no. 3, pp. 1247-1261.
18. Kumar, D., Seetharam, R. and Ponappa, K. (2024). Effects of graphene nano particles on interfacial microstructure and mechanical properties of Al7150/B4C hybrid nanocomposite fabricated by novel double ultrasonic two stage stir casting technique. *Journal of Alloys and Compounds*, vol. 1008, pp. 1766-1778.
19. Vishnoi, M., Srivastava, S., Rai, S., Verma, N. and TG, M. (2024). Experimental investigations of AA6061/Al2O3/WC/SiC hybrid metal matrix composite fabricated by two steps stir casting. *Advances in Materials and Processing Technologies*, vol. 10, no. 3, pp. 2374-2396.
20. Yan, D., Yang, H., Shan, Z., Xu, J., Yang, G. and Yin, Y. (2025). The Influence of the Composite Process of Sand Mold Additive Manufacturing and Low-Temperature Treatment on the Macro-and

Micro-Properties of A356 Aluminum Alloy for Aircraft Thin-Walled Cabins. *International Journal of Metal casting*, pp. 1-16.

21. Pardeshi, S., Barve, S., Pesode, P. and Gupta, N. (2026). Stir Casting of Aluminum Metal Matrix Composite for Automobile Application a Review. *Surface Review and Letters*, vol. 33, no. 5, pp. 250-268.
22. American society for testing and materials, ASTM E8/E8M (2024). Standard test methods for tension testing of metallic materials, west Conshohocken, pp. 157-177.
23. American society for testing and materials, ASTM E23 (2024). standard test methods for notched bar impact testing of metallic materials, west Conshohocken, pp. 231-247.
24. Elhadi, A., Amroune, S., Slamani, M., Jawaid, M., Koklu, U. and Bidi, T. (2024). Evaluation of drilling by induced delamination of hybrid biocomposites reinforced with natural fibers: a statistical analysis by RSM. *Journal of Composite Materials*, vol. *58*, no. 23, pp. 2515-2530.
25. Pankaj, Jawalkar, C.S., Kant, S., Khatkar, S.K. and Kumar, R. (2024). Natural frequency response simulation and mathematical modelling of nettle fiber-based composites using RSM process. *International Journal of Materials and Product Technology*, vol. 68, no. 3-4, pp. 316-329.
26. Nuru, Z.K., Elsaigh, W.A. and Kearsley, E.P. (2025). Characteristics of Laterite Soil for Potential Geopolymer Applications. *Minerals*, vol. 15, no. 7, pp. 19-741.
27. ISO 22412 (2017), Particle size analysis-dynamic light scattering (DLS). International Organization for Standardization. *Geneva, Switzerland*, pp. 76-91.
28. ASTM E3247-20 (2020). Standard test method for measuring the size of nanoparticles in aqueous media using dynamic light scattering, pp. 192-226.
29. Odiwo, H., Bello, K.A., Abdulwahab, M., Adebisi, A.A., Abdullahi, U., Dodo, R.M., Maleque, M.A. and Suleiman, M.U. (2023). Study on the Optimization of Surface Modification Processing of SiC_p and Tribological Properties of AA6061-SiCp based Composites. *International Journal of Engineering Materials and Manufacture*, vol. 8, no. 1, pp. 1-12.
30. Prasomthong, S., Phatungthane, T. and Chomchalao, C. (2025). Optimization of aluminium matrix composite production in a friction stir process with MgO nanoparticle reinforcement using ANN-GRA modelling. *Engineering and Applied Science Research*, vol. *52*, no. 3, pp. 282-295.
31. Kelsy, B.T., Nwobi-Okoye, C.C., Ezechukwu, V.C. and Uche, R. (2025). Multi objective optimization of novel Al-Si-Mg nanocomposites: a Taguchi-ANN-NSGA-II approach. *Journal of Engineering Research*, vol. 13, no. 1, pp. 267-282.
32. Aigbodion, V.S. and Ezema, I.C. (2019). Multifunctional A356 alloy/ PKSAnp composites: *Microstructure and Mechanical Properties, Defence Technology*, pp. 1-5. https://doi.org/10.1016/j.dt.2019.05.017.
33. Akinwande, A.A., Adesina, O.S., Adediran, A.A., Balogun, O.A., Mukuro, D., Balogun, O.P., Tee, K.F. and Kumar, M.S. (2023). Microstructure, Process Optimization, and Strength Response Modelling of Green-Aluminium-6061 Composite as Automobile Material. *Ceramics*, vol. 6, pp. 386-415.
34. Bayraktar, E. (2025). Recycle of Aluminium (A356) for Processing of New Composites Reinforced with Magnetic Nano Iron Oxide and. In *Mechanics of Composite and Multi-functional Materials, Volume 7: Proceedings of the 2016 Annual Conference on Experimental and Applied Mechanics, CRC Press*, pp. 313-327.
35. Tiwan, T., Nurhadiyanto, D., Mujiyono, M. and Restadi, F.A. (2025). Performance Improvement of A356 Cast Aluminium Alloy by Adding TiO2 Powder and Stirring in Microstructure and Strength. *Periodica Polytechnica Mechanical Engineering*, vol. 69, no. 3, pp. 204-214.